PROCEEDINGS OF SCIENCE

Open b and $b\bar{b}$ cross-section measurements using inclusive and exclusive channels at ATLAS

Ilektra Athanasia CHRISTIDI on behalf of the ATLAS collaboration[*†]
University College London
E-mail: electra.christidi@cern.ch

The production of b-quarks in proton-proton collisions at the LHC provides an important test of perturbative QCD. The cross-section can either be measured inclusively, using all tagged b-jets, or exclusively, exploiting specific B-hadron decay final states. This note describes measurements of the inclusive b-jet and $b\bar{b}$ production cross-sections and of the inclusive $B \to J/\psi X$ cross-section, and the observation of the exclusive channels $B^{\pm} \to J/\psi K^{\pm}$, $B_d \to J/\psi K^{0*}$ and $B_s \to J/\psi \phi$ performed with the ATLAS detector.

The 13th International Conference on B-Physics at Hadron Machines
April 4-8 2011
Amsterdam, The Netherlands

[*]Speaker.

[†]This work was supported in part by the EU Marie Curie program under the ERG "Higgs-ZAP" (contract number PERG05-GA-2009-249239) and the RTN "ARTEMIS" (contract number MRTN-CT-2006-035657), and the UK Science and Technology Facilities Council (STFC).

PoS(BEAUTY 2011)009

1. Introduction

The measurement of the inclusive jet and di-jet cross-sections with *b*-quark content tests theory predictions and is the first step in understanding other processes involving the production of *b*-quarks. For example, processes like *b*-jets produced in association with W or Z bosons represent substantial backgrounds in many searches for new physics at the LHC.

On the other hand, exclusive *B*-hadron cross-sections offer a cross-check and additional comparisons with hard-scatter models. Certain *B*-hadron decay channels can be used as references for rare, more interesting *B*-decays, therefore their exclusive cross-section is of particular interest.

2. Detector and tools overview

The most important parts of the ATLAS detector for measurements involving *b*-jets and hadrons are the Inner Detector (ID) and the Muon Spectrometer (MS). The former because precise tracking near the interaction point is crucial for identifying the *b* decay products, and the latter because, in studies with *b*-jets containing J/ψ 's, the final products of the J/ψ are a muon pair. More details about the ATLAS detector and its performance can be found in Ref. [1].

The ID consists of detectors of three different technologies for optimal position measurement and track reconstruction and it is immersed in a 2T solenoid magnetic field. The momentum scale measured in the ID is accurate to about 0.1% at low energy and about 1% up to 100 GeV, where alignment becomes the dominant effect. The primary-vertex resolution is $\mathscr{O}(10\mu\mathrm{m})$.

The MS consists of chambers of four different technologies for optimal muon reconstruction and triggering and it is immersed in a toroid magnetic field with an average strength of 0.5 T. The muon reconstruction efficiency is almost 100% for $p_T > 4-6$ GeV and the fake rate is $\sim$0.1%, and they have been both measured with data-driven methods. The momentum resolution for 50 GeV muons is $\sim$5%. For details about the muon reconstruction and its performance, see Ref. [2].

Muon tracks are first reconstructed in the MS and then extrapolated to the ID, where they are combined with an ID track. These are the best-quality muons ("combined"). In order to increase efficiency, reconstruction can start from a track in the ID, which is then combined with a track segment in the first station of the MS to create the "tagged" muons. Both those two reconstruction approaches have been used in the following analyses.

2.1 Track-based *b*-tagging

The track-based *b*-jet identification (*b*-tagging) relies on the long lifetime of *B* hadrons. In particular, secondary-vertex-based algorithms explicitly try to reconstruct the vertex of the *b*-decay. The algorithm used here ("SV0") starts from two-track vertices and the signed decay-length significance is its b-tag weight of the jet.

The tracking performance is crucial for *b*-tagging. It can be seen in Fig. 1 and Ref. [3] that the transverse impact parameter significance (d_o/σ_{d_o}), which is the most important quantity for track-based *b*-tagging, is in pretty good agreement with Monte Carlo simulation (MC). The agreement for low track p_T's shows a good understanding of the detector material, whereas the slight disagreement at higher p_T's is due to residual misalignment which is constantly being improved.

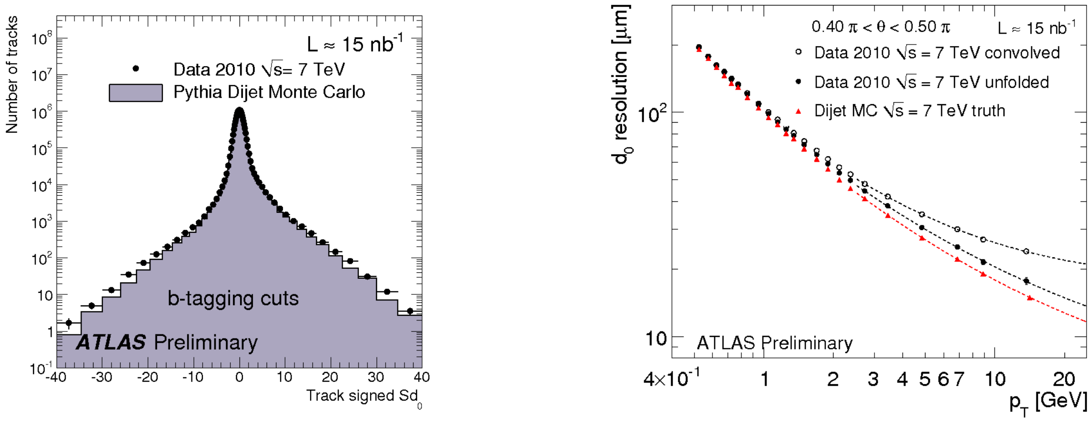

Figure 1: Transverse impact parameter (d_o) significance signed with respect to the jet axis (left) and its resolution as a function of track p_T convolved and de-convolved with the primary-vertex resolution (right) for data and MC.

The SV0 b-tagging efficiency has been measured with the data-driven p_T^{rel} method [4]. First jets containing one or more muons are selected, which are naturally enhanced in b, independent of any track-based b-tagging. Then the relative p_T of the muon with respect to the jet axis (p_T^{rel}) can be used to differentiate between light, c and b jets. The amount of b-jets is measured by a fit of the data to different templates derived either from data (for light jets) or MC (for c and b jets). Then the ratio of b-jets found by this fit after and before the SV0 cut is applied is the b-tagging efficiency. As a closure test of this calibration method, the SV0 decay length significance for data and for calibrated MC is shown in Fig. 2.

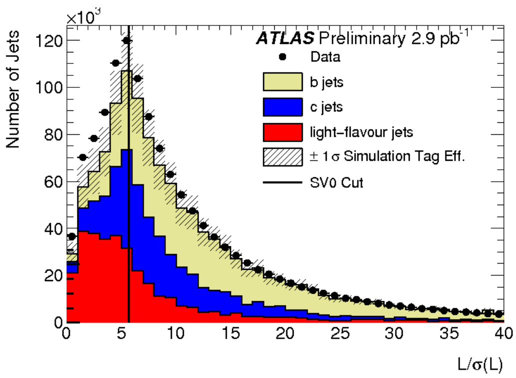

Figure 2: SV0-based decay-length significance: data and MC comparison, after correcting the MC with the data-driven tagging efficiency and mis-tag rate.

3. Inclusive b and $b\bar{b}$ cross-section

For the calculation of the inclusive b and $b\bar{b}$ cross-section, jets reconstructed with the anti-k$_T$ algorithm [5] and corrected to the Jet Energy Scale and for the muon and neutrino energy are used. The SV0 tagger is used to identify b-jets, then the efficiency correction derived with the p_T^{rel} method

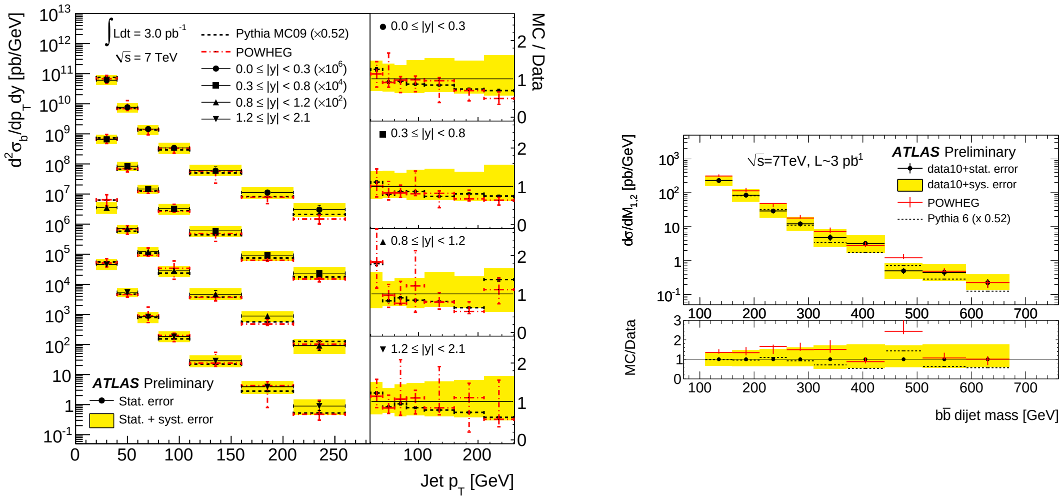

Figure 3: Inclusive double-differential b-jet cross-section as a function of jet p_T for different y's (left) and inclusive differential $b\bar{b}$ cross-section as a function of the di-jet invariant mass for b-jets with p_T >40 GeV and $|y| < 2.1$ (right). Both cross-sections are compared with LL and NLO MC.

is applied. The fraction of b (di-)jets in the final sample is derived from a binned log-likelihood fit of the secondary-vertex (SV) mass distribution to MC templates (the sum of the SV masses of the two jets for the case of di-jets). The double-differential inclusive b-jet cross-section (with respect to transverse momentum p_T and rapidity y) and the differential inclusive $b\bar{b}$ cross-section (with respect to di-jet mass M) are given by

$$\frac{d^2\sigma_b}{dp_T dy} = \frac{1}{\Delta p_T \Delta y}\frac{N_b \cdot frac_b}{\varepsilon_{trig}\cdot\varepsilon_{sel}\cdot\varepsilon_{btag}\cdot L}\times C$$
$$\frac{d\sigma_{b\bar{b}}}{dM} = \frac{1}{\Delta M}\frac{N_{b\bar{b}} \cdot frac_b}{\varepsilon^{jj}_{trig}\cdot\varepsilon^{jj}_{sel}\cdot\varepsilon^{jj}_{btag}\cdot L}\times C$$

where $N_{b(\bar{b})}$ is the number of SV0-tagged (di-)jets, $frac_b$ the fraction of them that are b (di-)jets found by the purity fit, $\varepsilon^{(jj)}_{trig}, \varepsilon^{(jj)}_{sel}, \varepsilon^{(jj)}_{btag}$ the (di-)jet trigger, selection and b-tagging efficiencies, L is the integrated luminosity and C is the bin-by-bin unfolding correction to particle level.

The results shown in Fig. 3 come from 3 pb^{-1} of data, for which single-jet and minimum bias triggers were used. The measurement is systematics dominated, with the Jet Energy Scale and the b-tagging efficiency and purity determination being the main sources of uncertainty. There is broad agreement with the Leading-Logarithm (LL) Pythia6 MC,as well as with Next-to-Leading-Order (NLO) POWHEG MC within the systematic uncertainties. Note that the Pythia6 prediction is rescaled by a factor 0.52, determined by normalizing the Pythia prediction to the same integrated cross-section as the measurement. More details can be found in Ref. [6].

4. $B \to J/\psi X$ cross-section

The inclusive $B \to J/\psi X$ cross-section is calculated by convolving the inclusive $J/\psi \to \mu^+\mu^-$ production cross-section with the non-prompt J/ψ fraction. The latter expresses the fraction of

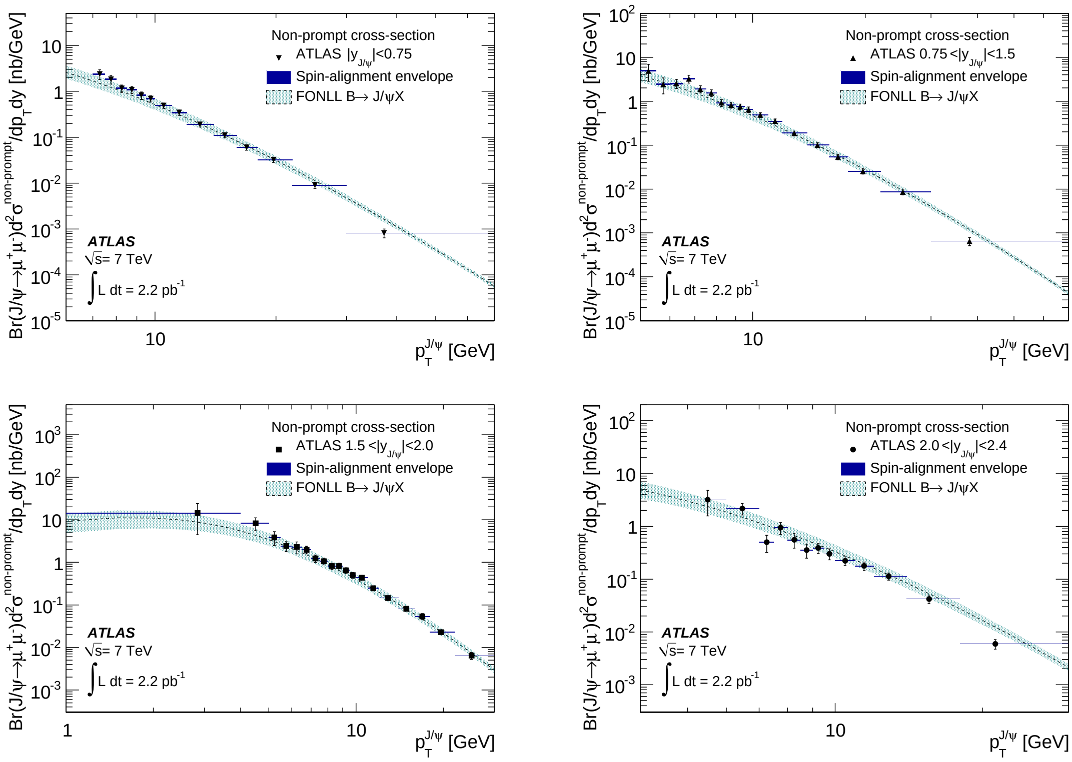

Figure 4: Non-prompt J/ψ production cross-section as a function of J/ψ p_T for different y regions, compared to predictions from FONLL theory. Overlaid is a band representing the variation of the result under spin-alignment variation on the non-prompt J/ψ component as described in Ref. [7].

J/ψ 's coming from the decays of long-lived particles such as B hadrons, as opposed to prompt mechanisms (QCD processes in which neither charm quark in the J/ψ comes from the decay of a B hadron). The measurement of the two components of the inclusive $B \to J/\psi X$ cross-section are described in the following chapters. More details can be found in Ref. [7]. The resulting non-prompt double-differential cross-section is shown in Fig. 4, and is in good agreement with the Fixed-Order-Next-to-Leading-Logarithm (FONLL) theoretical prediction.

4.1 Inclusive $J/\psi \to \mu^+\mu^-$ cross-section

For the measurement of the inclusive J/ψ cross-section, events with at least two muons are selected, at least one of which is MS-ID combined. The ID tracks associated to those muons are fitted to a secondary vertex and the opposite-charge di-muon invariant mass is recomputed. Each J/ψ candidate is multiplied by a correction factor ω in order to estimate the true number of $J/\psi \to \mu^+\mu^-$ decays that occured, with ω given by

$$\omega^{-1} = A \cdot M \cdot \varepsilon_{trk}^2 \cdot \varepsilon_{\mu 1} \cdot \varepsilon_{\mu 2} \cdot \varepsilon_{trig}$$

where A is the acceptance that depends on the kinematics, the detector geometry and the production model (J/ψ polarization), M the bin migration correction and $\varepsilon_{trk}^2, \varepsilon_{\mu 1/2}, \varepsilon_{trig}$ the ID tracking, muon reconstruction and trigger efficiency.

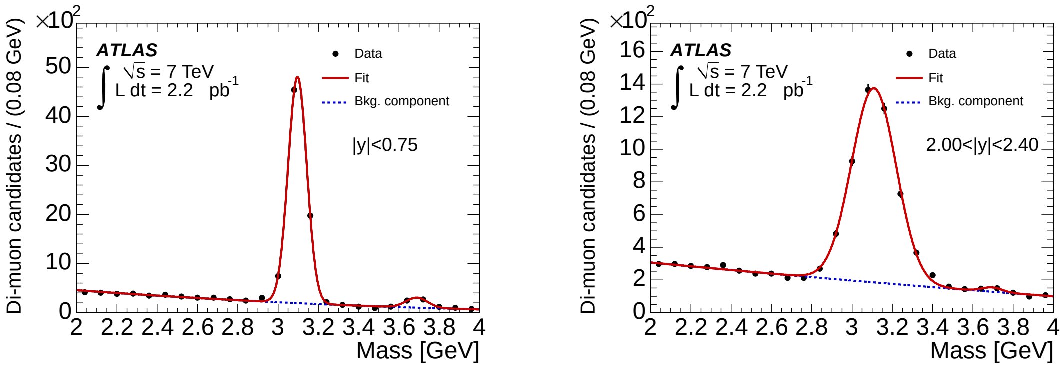

Figure 5: Invariant-mass distributions of reconstructed J/ψ candidates used in the cross-section analysis with fit results, for the most central and the most forward y regions.

This acceptance and efficiency-corrected di-muon-mass distribution is then fitted in a binned minimum χ^2 fit to get the J/ψ mass, mass resolution and number of signal events, as well as the background normalization and slope. The J/ψ signal is modeled by a Gaussian, and the background by a straight line. The results of this fit in the most central and most forward y region are shown in Fig. 5 for 2.27 pb^{-1} of data, where single-muon and minimum-bias triggers were used.

4.2 J/ψ non-prompt fraction

The discriminant between prompt and non-prompt J/ψ 's is the pseudo-proper time $\tau = \frac{L_{xy} m^{J/\psi}}{p_T^{J/\psi}}$, where L_{xy} is the signed projection of the J/ψ flight distance onto its p_T. A simultaneous unbinned maximum-likelihood fit is performed in di-muon mass and pseudo-proper time, in order to get the J/ψ mass and resolution, the J/ψ signal fraction, the non-prompt J/ψ fraction and the pseudo-proper time slope and resolution. The result of such a fit is shown in Fig. 6 for a given p_T and y bin. The signal pseudo-proper time model is derived from candidates in the mass-peak region [2.9,3.3] GeV shaded in red, and the background one from the mass sidebands outside this region, shaded in blue. They both contain a prompt and a non-prompt component.

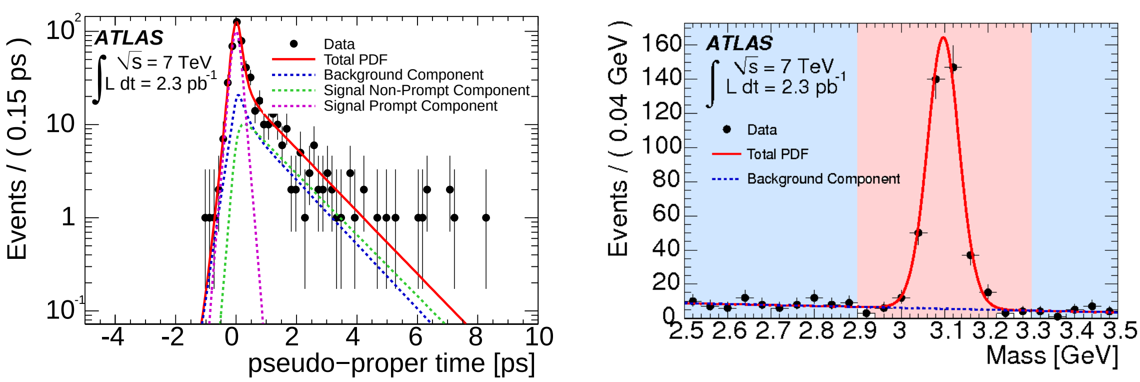

Figure 6: Pseudo-proper time distribution of $J/\psi \rightarrow \mu^+\mu^-$ candidates in the signal mass region for a given p_T bin (9.5 GeV< p_T <10.0 GeV) in the most central rapidity region, with fit results (left). Di-muon invariant mass distribution which is simultaneously fitted with the pseudo-proper time for the same bins (right).

The non-prompt to inclusive J/ψ fraction $f_B = \frac{d\sigma(pp\to B+X\to J/\psi+X')}{d\sigma(pp\to J/\psi+X'')_{inc}}$ as a function of p_T for the four different y regions can be found in Ref. [7].

5. Exclusive B decays

The exclusive decays of B hadrons to J/ψ plus light mesons offer a variety of interesting measurements: exclusive B-hadron lifetimes and differential production cross-sections, double lifetimes and helicity amplitudes in the case of mixing, detector performance tests. Moreover, they serve as a reference to rare B-decays branching ratio measurements. For all those measurements, the observation of the exclusive decays reported here is the first step.

5.1 $B^\pm \to J/\psi K^\pm$ observation

For the detection of $B^\pm \to J/\psi K^\pm$ decays, a di-muon in the J/ψ mass range is combined with a third track with the kaon mass assigned. Then all three tracks are fitted to a common vertex, with the J/ψ mass constraint on the di-muon. The background is further suppressed by requiring a transverse decay length $L_{xy} > 0.3$ mm. The $B^\pm$ mass and number of candidates are extracted by an unbinned maximum-likelihood fit on the three-track mass, where the signal is modeled with a Gaussian and the background with a straight line. The result of this fit is shown in Fig. 7 for 3.4 pb^{-1} of data, where single- and di-muon triggers were used. The $B^\pm$ mass found is in good agreement with the PDG value. The excellent agreement between B^+ and B^- results shown in the same figure prove a good understanding of the detector. More details can be found in Ref. [8].

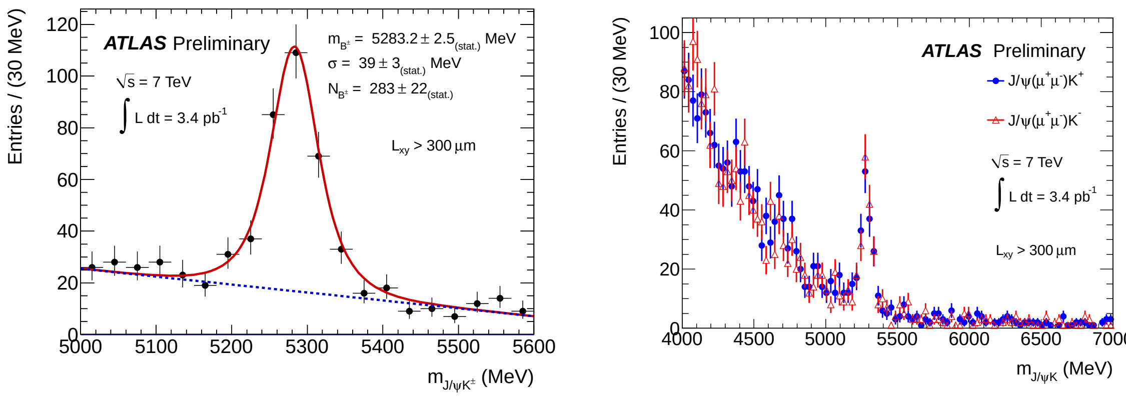

Figure 7: Invariant-mass distributions of reconstructed $B^\pm \to J/\psi K^\pm$ candidates with fit results (left) and of B^+ and B^- candidates separately (right).

5.2 $B_d \to J/\psi K^{0*}$ and $B_s \to J/\psi \phi$ observation

For the detection of $B_d \to J/\psi K^{0*}$ and $B_s \to J/\psi \phi$ decays, a di-muon in the J/ψ mass range is combined with two other tracks with the appropriate mass assignments and constraints. The $B_{d/s}$ mass and number of candidates are extracted by an unbinned maximum-likelihood fit on the four-track mass, where the signal is modeled with a Gaussian and the background with a line. The result of this fit is shown in Fig. 8 for 40 pb^{-1} of data, where a cut on the decay time has also been applied to further suppress the background. More details can be found in Ref. [9].

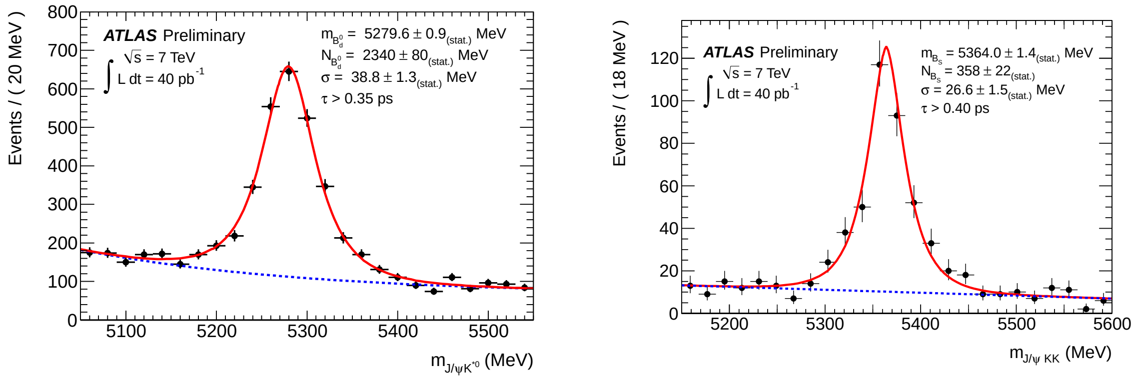

Figure 8: Invariant-mass distributions of reconstructed $B_d \to J/\psi K^{0*}$ (left) and $B_s \to J/\psi\phi$ candidates (right) with fit results.

6. Conclusions

The most up-to-date ATLAS measurements of the inclusive and exclusive B cross-sections have been presented. The first ATLAS b-jet and $b\bar{b}$ cross-section results show good agreement with LL and NLO MC. The $B \to J/\psi X$ inclusive cross-section is also in agreement with FONLL predictions and other experiments. A number of exclusive $B \to J/\psi K$ channels have been observed and show an excellent understanding of the detector. This bodes well for cross-section and lifetime measurements, as well as searches for and measurements of rare decays.

References

[1] The ATLAS collaboration, *The ATLAS Experiment at the CERN Large Hadron Collider*, JINST **3** (2008) S08003; R. Nikolaidou, *ATLAS Detector Performance*, in these proceedings.

[2] M. Corradi, *Di-muon Reconstruction for B-physics in ATLAS*, in these proceedings.

[3] The ATLAS collaboration, *Tracking Studies for b-tagging with 7 TeV Collision Data with the ATLAS Detector*, ATLAS-CONF-2010-070.

[4] The ATLAS collaboration, *Calibrating the b-Tag Efficiency and Mistag Rate of the SV0 b-Tagging Algorithm in 3pb^{-1} of Data with the ATLAS Detector*, ATLAS-CONF-2010-099.

[5] M. Cacciari, G. P. Salam, and G. Soyez, *The anti-k_t jet clustering algorithm*, *JHEP* **04** (2008) 063.

[6] The ATLAS collaboration, *Measurement of the Inclusive and Di-jet Cross Sections of b-jets in pp collisions at $\sqrt{s} = 7$ TeV with the ATLAS detector*, ATLAS-CONF-2011-056.

[7] The ATLAS collaboration, *Measurement of the differential cross-sections of inclusive, prompt and non-prompt J/ψ production in proton-proton collisions at $\sqrt{s} = 7$ TeV*, hep-ex/1104.3038v1; S.-C. Hsu, *J/ψ Production in pp and in Heavy-Ion Collisions in ATLAS*, in these proceedings.

[8] The ATLAS collaboration, *Observation of the $B^{\pm}$ meson in the decay $B^{\pm} \to J/\psi(\mu^+\mu^-)K^{\pm}$ in ATLAS*, ATLAS-CONF-2010-098.

[9] The ATLAS collaboration, *Observation of the B_d^0 and B_s^0 mesons in the decays $B_d^0 \to J/\psi K^{0*}$ and $B_s^0 \to J/\psi\phi$ in ATLAS*, ATLAS-CONF-2011-050; A. Dewhurst, *$B_s \to J/\psi\phi$ decays in ATLAS*, in these proceedings.